Applied Catalysis B: Environmental 331 (2023) 122678

Contents lists available at ScienceDirect

Applied Catalysis B: Environmental

journal homepage: www.elsevier.com/locate/apcatb

Highly active and water-resistant Lanthanum-doped platinum-cobalt oxide catalysts for CO oxidation

Liuxin Xu, Ya Pan, Hongmei Li, Ruichao Xu, Zhihu Sun *

National Synchrotron Radiation Laboratory, University of Science and Technology of China, Hefei 230029, PR China

ARTICLE INFO

Keywords:
CO oxidation
Water resistance
Pt-CoO catalysts
La-doping
Metal-oxide interfaces
In situ characterizations

ABSTRACT

The presence of interfacial sites between Pt-group metals and transition metal oxides can effectively improve the catalytic activity of Pt-group catalysts, but under moisture-rich conditions they suffer from severe deactivation due to water poisoning of the active sites. Here, we propose for the first time a Lanthanum (La)-doping strategy to improve the water-resistance of the Pt-based catalysts. We synthesized a Pt-CoO/Al_2O_3 catalyst that is active for CO oxidation under dry conditions but deactivates rapidly under moisture. This rapid deactivation is overcome by La-doping, which delivers boosted activity (100 % CO conversion at — 15 °C) and long-term on-stream stability. In situ X-ray absorption fine-structure and in situ diffuse reflectance infrared Fourier transform spectra revealed that the doped La, in the form of La_2O_3, plays dual roles of suppressing the carbonate formation on the active sites and modifying the electronic structure of Pt. The synergetic effects between La_2O_3 and the active Pt−O−Co interfacial sites in La-doped Pt-CoO/Al_2O_3 lead to the outstanding activity under the moisture-rich condition.

1. Introduction

Platinum group metals (PGMs) catalysts supported on metal oxides are widely applied to heterogeneous catalysis because of their high activity, selectivity and stability, such as CO oxidation [1–5], propane dehydrogenation [6–9] and water-gas shift [10–13]. In heterogeneous catalysis systems, CO oxidation plays key roles in both surface catalytic systems as a probe reaction and in environmental-related applications including air cleaning and automobile exhaust gas treatment [14,15]. However, the PGM catalysts have dissatisfactory catalytic ability at low temperatures (< 100 °C) [16] because the strongly chemisorbed CO inhibits the dissociative adsorption of O_2 and poisons the reaction active sites [17,18]. In recent decades, multiple efficient strategies to suppress CO poisoning in the PGM catalytic systems have been proposed, via decreasing the metal sizes [19], alloying [20–23], or constructing the metal-oxide interface [5,24–28], and so forth. Especially, the metal-oxide interfaces between PGM and transition metal (TM) oxides (FeO, CoO, NiO_x) [21,27,29] have attracted extensive attention in improving the performance for CO oxidation, where the TM oxides provide the active sites for oxygen activation.

In realistic environments, however, the process of CO oxidation inevitably involves water vapor, and water often causes deactivation of metal oxide interfacial sites [30,31]. Many PGM-TM oxide interfaces are merely applied to CO oxidation under dry environment [29,32–34], because water molecules can be readily adsorbed on the TM oxides and dissociated therein to produce hydroxyl species that poison the catalytic active sites [35,36]. In addition, H_2O can accelerate the formation of carbonate species that block the metal active sites, and deactivate the catalysts [37,38]. Hence, seeking robust catalysts with high activity and water-resistance ability is greatly significant for low-temperature CO catalytic oxidation under moisture-rich conditions, especially in environment-related applications. Numerous studies have been performed to enhance the water resistance of PGM-oxide interfaces. For instance, Zhu et al. [39] used the spinel oxides MFe_2O_4 (M = Ni and Co), instead of the monometallic oxides of Fe_3O_4, CoO, NiO, as supports to anchor the Pt catalysts. Due to the interactions between Pt and spinel oxides, the Pt/MFe_2O_4 catalysts show better activity and water tolerance than Pt metals supported on monometallic oxides under wet reaction conditions. Another way is to use the strong metal−support interactions (SMSI) between PGM and TM oxide supports, as exemplified by the work by Wu et al. [40]. They designed PtCo/Co_3O_4-SiO_2 catalysts where the SMSI between PtCo nanoalloys and Co_3O_4-SiO_2 supports can create lots of active lattice oxygen to improve the catalytic performance for CO oxidation in water vapor and render structural stability. In spite of these

* Corresponding author.
E-mail address: zhsun@ustc.edu.cn (Z. Sun).

https://doi.org/10.1016/j.apcatb.2023.122678
Received 17 December 2022; Received in revised form 21 February 2023; Accepted 22 March 2023
Available online 23 March 2023

progresses, the formation of water-induced carbonate and hydroxyl species which lead to the metal-oxide interfaces poisoning is still inevitable under moisture-rich conditions.

Recent studies have shown that rare-earth oxides are inherently hydrophobic due to their special electronic structures of surfaces, and hence bonds with water could be hardly formed on the rare-earth oxide surface [41,42]. Therefore, it can be expected that the addition of rare-earth oxides might decrease the poisonous effects on the PGM-TM oxides interfaces. In this work, we report for the first time a Lanthanum (La)-doping strategy to improve the water-resistance of the Pt-based catalysts. We synthesized La-doped Pt-CoO/Al_2O_3 catalysts by the co-deposition method in colloidal solutions, which exhibit boosted catalytic performance against water-induced deactivation. In situ X-ray absorption fine-structure (XAFS) spectroscopy and in situ diffuse reflectance infrared Fourier transform (DRIFT) spectroscopy were combined to investigate the structural properties and surface species when the catalysts were exposed to the wet CO oxidation (COOX) reaction condition. It is revealed that the enhanced activity and water resistance of the La-doped Pt-CoO/Al_2O_3 catalyst was attributed to the addition of La_2O_3, which significantly inhibits the formation of carbonate species on the Pt−O−Co interfaces. This work demonstrates that La_2O_3 or possibly other rare earth oxides is an important category of additives to enhance water resistance on metal-oxide interfaces, and could provide an effective method to design water-resistant catalysts for practical applications.

2. Experimental section

2.1. Chemicals and materials

Chemicals and materials. Cobalt nitrate hexahydrate, chloroplatinic acid hexahydrate, sodium hydroxide and ethylene glycol (EG) were purchased from Sinopharm Chemical Reagent Co. Ltd. Lanthanum nitrate hexahydrate and Aluminum oxide were purchased from Aladdin. All chemicals and materials were kept under ambient temperature and used without any further purification.

2.2. Synthesis of Lanthanum (La)-doped Pt-CoO-Al_2O_3 catalysts

The synthesis of Lanthanum (La)-doped Pt-CoO/Al_2O_3 was divided into two steps. The synthesis procedure of 0.2La-Pt-CoO/Al_2O_3 is taken as an instance. Firstly, the 0.2La-Pt-CoO nanoparticles were prepared by modifying the established method [43]. 0.084 g of $La(NO_3)_3{\cdot}6\ H_2O$, 0.281 g of $Co(NO_3)_2{\cdot}6\ H_2O$ and 0.5 g of $H_2PtCl_6{\cdot}6\ H_2O$ were dissolved in 25 mL of ethylene glycol (EG) into a 100 mL three-necked flask. After that, 25 mL of 0.5 M NaOH in ethylene glycol was added with stirring to obtain the colloidal solution. The reaction mixture was rapidly heated to 140 °C for 3 h under a flowing Ar atmosphere and followed by cooling to room temperature. Then, the dark-brown colloids were obtained, suggesting the formation of nanoparticles (NPs) with a nominal La: Pt: Co molar ratio of 0.2:1: 1, and the sample was named 0.2La-Pt-CoO. Secondly, 4.05 mL of the as-synthesized 0.2La-Pt-CoO colloids was added into 50 mL of EG in a 100 mL round-bottom flask. Subsequently, 0.5 g γ-Al_2O_3 supports were added into the solution and thoroughly mixed under stirring at 80 °C for 3 h, and the pH value of the mixture was adjusted to around 9 by dropwise addition of 0.5 M NaOH/EG solution. After that, the resulting precipitate was filtered with the mass ultra-pure water to remove the chlorine residues, and then the samples were dried in air at 80 °C for 12 h to obtain the supported 0.2La-Pt-CoO/Al_2O_3 catalyst. 0.4La-Pt-CoO/Al_2O_3 samples were synthesized by using the same method while varying the amount of $La(NO_3)_3{\cdot}6\ H_2O$ precursor. The Pt-CoO/Al_2O_3 was synthesized using the same method without addition of $La(NO_3)_3{\cdot}6\ H_2O$, and similarly, the Pt/Al_2O_3 catalyst was synthesized using the same method with only Pt colloids.

2.3. Catalytic activity test

The activities of catalysts for CO oxidation were tested using a U-shaped quartz fixed-bed reactor tube with 50 mg of the catalyst under atmospheric pressure and a wet reaction condition. The sample was pretreated at 100 °C in a flow of 10 vol% O_2/Ar for 1 h and reduced by 10 vol% H_2/Ar at 200 °C for 1 h, and then the catalyst was cooled down to room temperature. The catalytic performance for CO oxidation was tested at a space velocity of 36,000 mL g^{-1} h^{-1} with a wet reaction gas consisting of 1 vol% CO, 1 vol% O_2, ~5 vol% H_2O/Ar (denoted as COOX). To accomplish the wet condition, the reaction gas passed through a bench-scale water bubbling reactor, and the water content (~5 % of water vapor) was regulated by controlling the temperature of the bubbler at 33 °C. The temperature of the activity test ranged from —30 to 200 °C. The gas compositions of the reactants and products in the inlet and outlet were analyzed by an online gas chromatograph (Shimadzu GC-2014) equipped with a thermal conductivity detector. The conversion of CO (denoted as X_{CO}) was calculated by the following equation:

$$X_{CO} = \frac{[CO]_{in} - [CO]_{out}}{[CO]_{in}} \times 100\%, \quad (1)$$

where $[CO]_{in}$ and $[CO]_{out}$ are the CO volumes in gas compositions of reactants and products, respectively. Kinetic measurements for the mass-specific rates, apparent activation energy (E_a), and reaction orders were conducted under the identical fixed-bed reactor. Decreasing the mass of catalysts and increasing the space velocity of the reaction gas was taken to ensure the CO conversion below 15 %. The specific rates of the mass (denoted as r_{CO}) were calculated using the following equation:

$$r_{CO}\left((\text{mol CO})h^{-1}\left(\text{g Pt}^{-1}\right)\right) = \frac{F_{co}X_{co}}{X_{Pt}m_{cat}}, \quad (2)$$

where F_{CO} is the CO gas flow rate in mol s^{-1}, X_{CO} is the CO conversion, X_{Pt} is the Pt loading, and m_{cat} is the catalyst mass.

2.4. Sample characterizations

The La, Pt and Co loading of the catalyst were determined by inductively coupled plasma-atomic emission spectrometry (ICP-AES, Optima 7300 DV) after dissolution with nitrohydrochloric acid for 1 h. Prior to the following characterizations, the samples were pre-reduced in 10 vol% H_2/Ar at 200 °C for 1 h. The X-ray diffraction (XRD) measurements were conducted on the Rigaku Miniflex-600 diffractometer equipped with a monochromatized Cu Kα radiation (λ = 1.5406 Å), operated at 40 kV voltage and 15 mA current. The X-ray photoelectron spectroscopy (XPS) measurements were performed on a Thermo ESCALAB 250Xi system using a monochromatic Al Kα (1486.6 eV) irradiation. The transmission electron microscopy (TEM) images of the samples were recorded at the JEM-2100 F instrument with an acceleration voltage of 200 kV. The high-angle annular dark-field scanning transmission (HAADF-STEM) measurements were conducted on the FEI Tecnai G2 F20 S-Twin high-resolution transmission electron microscope under the aberration correction mode operated at 200 kV. The energy-dispersive X-ray (EDX) mapping images were taken using a JEOL JEM-ARM200F TEM/STEM electron microscope with 300 kV.

2.5. In situ DRIFTS

In situ DRIFTS experiments were conducted at the BL01B beamline at National Synchrotron Radiation Laboratory (NSRL), Hefei, China, using a Bruker IFS 66 v/s Fourier-transform infrared spectrometer, equipped with a diffuse reflectance accessory and a liquid nitrogen-cooled HgCdTe detector and operated at a resolution of 4 cm^{-1} for 128 scans, and the DRIFTS spectra were measured in the 3000–1000 cm^{-1} wavenumber range. Prior to each experiment, the samples mixed with KBr were reduced in 10 vol% H_2/Ar at 200 °C for 30 min in the in-situ DRIFTS cell. The high-purity Ar was used to remove the residual H_2, followed by cooling to room temperature, and then the background spectrum was collected in the flowing Ar atmosphere. After obtaining the background spectrum, the continuous DRIFTS spectra were collected

under the different gas atmospheres, consisting of 1 vol% CO/Ar or wet COOX (1 vol% CO, 1 vol% O_2, ~5 vol% H_2O/Ar), respectively. The rates of all the gas flows involved were 30 mL/min.

2.6. In situ XAFS

In situ XAFS measurements were conducted at the BL14W1 beamline of the Shanghai Synchrotron Radiation Facility (SSRF), China. The storage ring was worked at 3.5 GeV with a maximum current of 210 mA under a top-up mode, with the Si (111) double-crystal monochromator. In situ Pt L_3-edge XAFS spectra for the samples were collected in the transmission mode, and in situ Co K-edge XAFS data were collected in the fluorescence mode. Prior to the measurements, all samples were pressed into 10 mm diameter pellets and loaded into the self-designed quartz reaction cell. The samples were reduced at 200 °C for 30 min in 10 vol% H_2/Ar and kept the rate of flow at 30 mL/min. Then the XAFS spectra were collected at the room temperature. Afterwards, the high-purity Ar was used to remove the residual H_2, and then the wet reaction gas (consisting of 1 vol% CO, 1 vol% O_2, ~5 vol% H_2O/Ar) was injected into the chamber (30 mL/min). After keeping the samples for 30 min, the XAFS spectra were recorded. The XAFS data were processed using the ATHENA module implemented in the IFEFFIT software packages [44], and the least-square curve-fitting was accomplished by using the ARTEMIS module [45] of IFEFFIT.

3. Results

3.1. Catalyst performance and reaction kinetics for CO oxidation

The catalysis performance of the Pt/Al_2O_3, Pt-CoO/Al_2O_3 and 0.2La-Pt-CoO/Al_2O_3 catalysts for CO oxidation were tested in the COOX atmosphere with or without water, at a space velocity of 36,000 mL g^{-1} h^{-1}. Under the dry condition, both the Pt-CoO/Al_2O_3 and 0.2La-Pt-CoO/Al_2O_3 catalysts are highly active, achieving 100 % CO conversion at 5 and —25 °C (Fig. S1 in the Supporting Information), respectively. In contrast, 100 % CO conversion could be reached on Pt/Al_2O_3 only when the temperature is higher than 150 °C. Under the wet COOX (containing ~5 % of water vapor) condition, the catalytic activity of the Pt/Al_2O_3 is not remarkably changed, while the activity of Pt-CoO/Al_2O_3 is significantly deteriorated (Fig. 1a). The complete CO conversion temperature on Pt-CoO/Al_2O_3 increases sharply from 5 °C under the dry COOX condition to 120 °C under the wet COOX condition, in agreement with previous studies that water deactivates the PGM-based catalysts [39,46,47]. Intriguingly, such a dramatic water-induced deactivation does not occur on the 0.2La-Pt-CoO/Al_2O_3 catalyst, which still achieves 100 % CO conversion at the cryogenic temperature of around —15 °C. Comparison of the catalytic activities under dry and wet conditions suggests the greatly improved water-resistance of La-doped Pt-CoO/Al_2O_3 catalysts for CO oxidation. Fig. 1b shows the long-term stability of catalysts with a space velocity of 200,000 mL g^{-1} h^{-1} at 20 °C under the wet COOX condition. After continuous 30 h of on-stream reaction, the CO conversion over the 0.2La-Pt-CoO/Al_2O_3 catalyst only declines slightly. In sharp contrast, the CO conversion on Pt-CoO/Al_2O_3 drops from 31 % to 9 % within 1 h, and further decreases to 2 % after 15 h of reaction. Additionally, after regeneration of the used 0.2La-Pt-CoO/Al_2O_3 catalyst at 200 °C by 10 vol% H_2/Ar for 1 h, the CO conversion could be largely restored (Fig. S2), indicating its good regenerability. These results demonstrate that La-doping into Pt-CoO/Al_2O_3 could remarkably enhance the water-resistance ability and catalytic stability while not sacrificing the catalytic activity for CO oxidation under the wet reaction condition. Nevertheless, further increasing the La content slightly decreases the catalytic performance (Fig. S3).

To further compare the intrinsic performance, the apparent activation energies (E_a) of the Pt/Al_2O_3, Pt-CoO/Al_2O_3 and 0.2La-Pt-CoO/Al_2O_3 catalysts were estimated. The Arrhenius plots in Fig. 1c show that

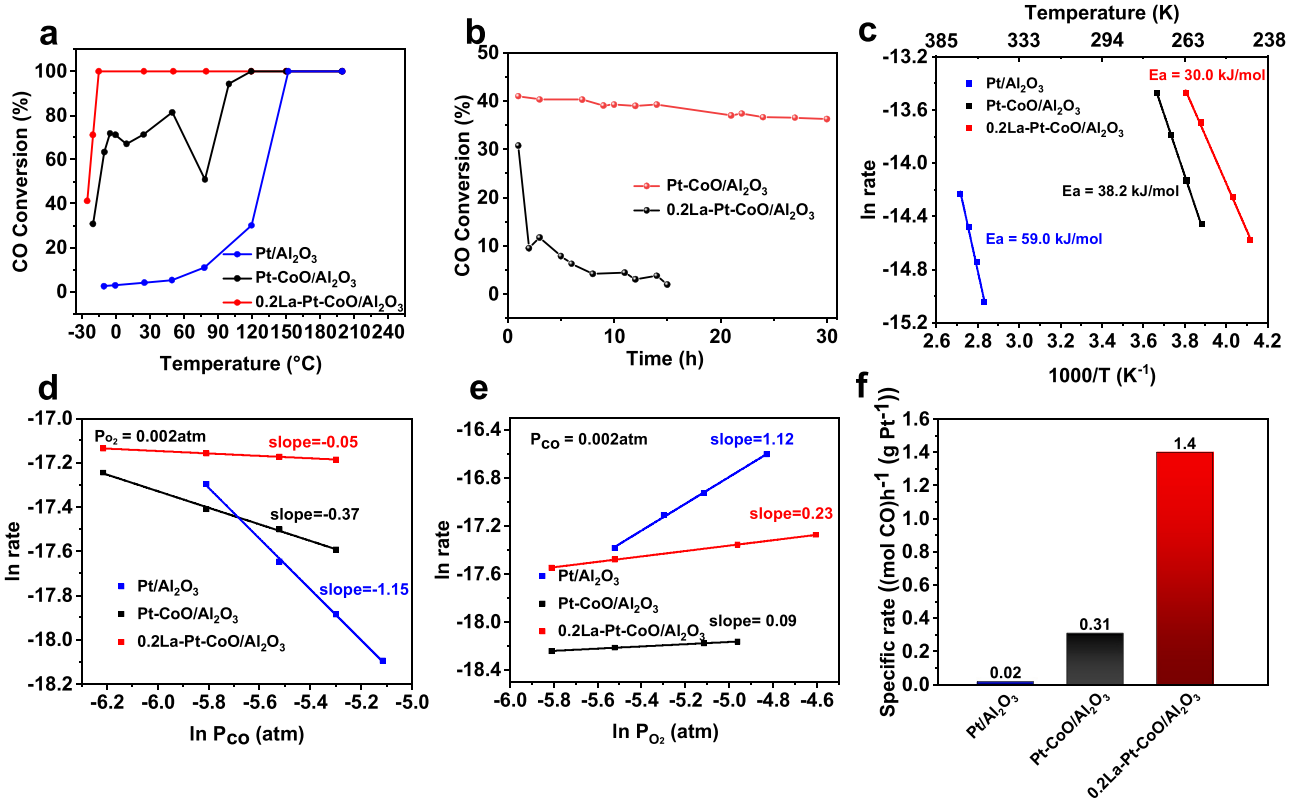

Fig. 1. (a) The CO conversion of various catalysts under the wet COOX condition (50 mg of catalyst mixed with 1.0 g quartz sand, 1 % CO, 1 % O_2, ~5 % water vapor balanced by Ar). (b) Long-term stability test at 20 ℃ under the wet COOX condition. (c) Apparent activation energies (E_a). Reaction orders of (d) CO and (e) O_2 for various catalysts. (f) Mass-specific reaction rates at the atmospheric pressure at 0 ℃.

the E_a of 0.2La-Pt-CoO/Al_2O_3 is 30.0 kJ/ mol, lower than those of Pt-CoO/Al_2O_3 (38.2 kJ/mol) and Pt/Al_2O_3 (59.0 kJ/mol). This suggests that La-doping into Pt-CoO/Al_2O_3 not only enhances the water-resistance ability, but also increases the intrinsic activity towards CO oxidation. Meanwhile, to shed some light on the CO oxidation mechanism, the CO and O_2 reaction orders of various catalysts were estimated and the results are shown in Fig. 1d-e. The reaction orders of CO and O_2 are —1.15 and 1.12 on Pt/Al_2O_3, respectively, consistent with the competitive Langmuir-Hinshelwood mechanism where adsorbed CO on the Pt particle surface inhibits O_2 activation. In contrast, the CO reaction order is —0.37 and —0.05 on Pt-CoO/Al_2O_3 and 0.2La-Pt-CoO/Al_2O_3, respectively. The increased reaction orders indicate that the CO poisoning effect is largely inhibited on Pt-CoO/Al_2O_3 and 0.2La-Pt-CoO/Al_2O_3, and the reaction mechanism thereon is different from that on monometallic Pt nanoparticles of Pt/Al_2O_3 (Fig. 1d). The mass-specific reaction rates were also evaluated at 0 °C within the kinetic control region. As shown in Fig. 1f, the specific rate for 0.2La-Pt-CoO/Al_2O_3 is 1.4 (mol CO) h^{-1} (g Pt) $^{-1}$, more than 4 times higher that of Pt-CoO/Al_2O_3 (0.31 (mol CO) h^{-1} (g Pt) $^{-1}$) and 70 times higher than that of Pt/Al_2O_3 (0.02 (mol CO) h^{-1} (g Pt) $^{-1}$). The above results indicate that the 0.2La-Pt-CoO/Al_2O_3 catalyst exhibits a greatly enhanced intrinsic activity for CO oxidation in the wet reaction condition.

3.2. Catalyst characterizations

In order to understand the different catalytic performance of the Pt/Al_2O_3, Pt-CoO/Al_2O_3 and 0.2La-Pt-CoO/Al_2O_3 catalysts, structure characterizations were performed. The transmission electron microscopy (TEM) images of the synthesized samples after H_2 reduction are given in Fig. 2a-b for Pt-CoO/Al_2O_3 and 0.2La-Pt-CoO/Al_2O_3, and in Fig. S3 for Pt/Al_2O_3. All these catalysts possess a similar average Pt particle size of 1.8–2.0 nm shown in the histogram of particle size distribution (inset in Fig. 2a-b, and Fig. S4). The XRD patterns (Fig. S5) only display the diffraction peaks of Al_2O_3, without any diffraction peaks of the Pt, La and Co species, in agreement with the small particle sizes of Pt nanoparticles (~2 nm) that cannot be detected by XRD. The actual loadings of La, Pt and Co were revealed by inductively coupled plasma atomic emission spectroscopy (ICP-AES) analysis, as shown in Table S1, indicating the similar Pt loading of 2.0–2.3 wt% for all samples. The Co loadings in Pt-CoO/Al_2O_3 (0.33 wt% Co) and 0.2La-Pt-CoO/Al_2O_3

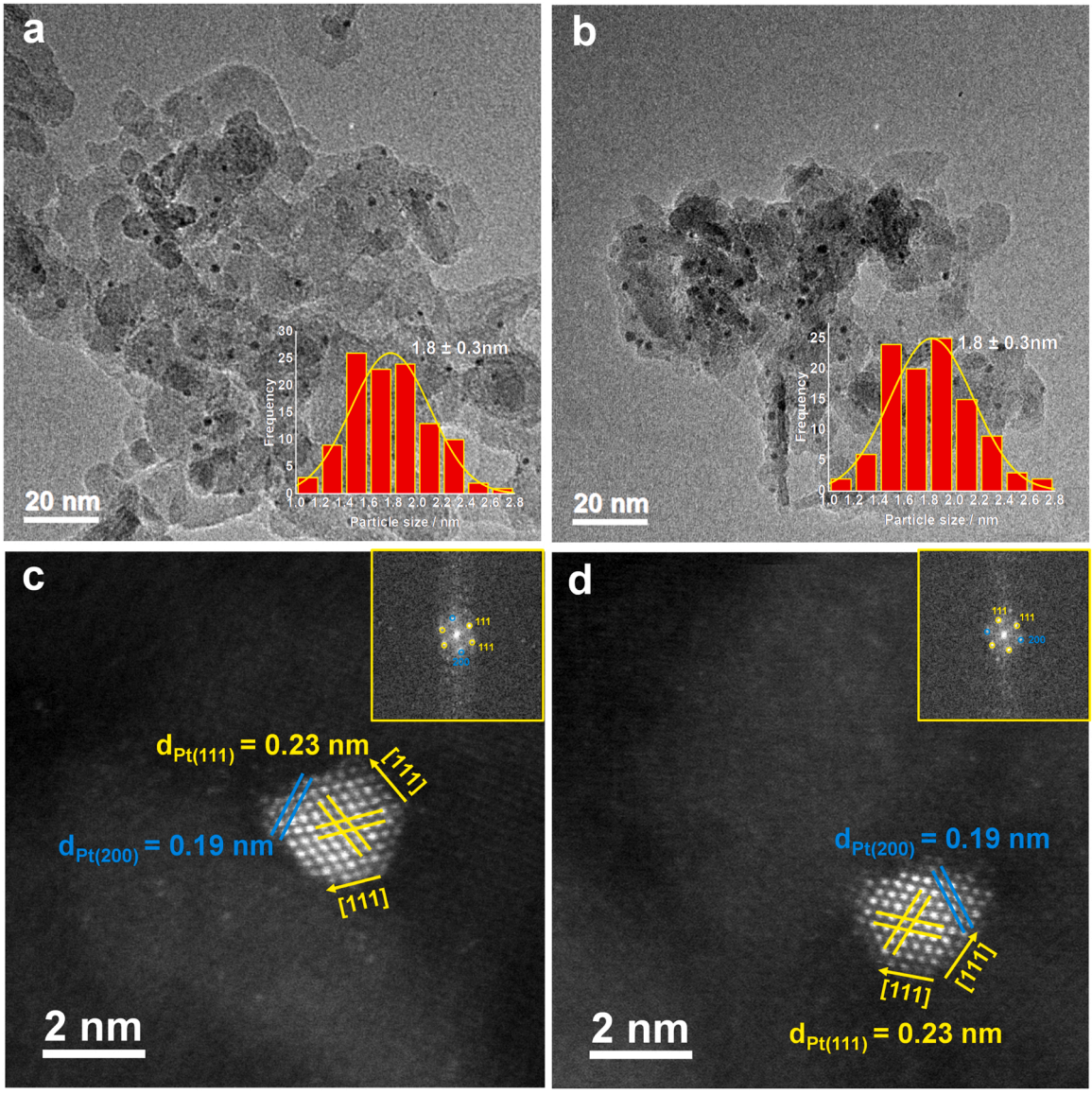

Fig. 2. TEM images and sizes distribution of (a) Pt-CoO/Al_2O_3, and (b) 0.2La-Pt-CoO/Al_2O_3. AC-HAADF-STEM images of (c) Pt-CoO/Al_2O_3, and (d) 0.2La-Pt-CoO/Al_2O_3. The insets in (c) and (d) are the corresponding FFT patterns.

(0.39 wt% Co) are also similar, with the even lower La loading of 0.21 wt% in 0.2La-Pt-CoO/Al_2O_3. Thus, the addition of a small amount of La and Co has negligible effects on the Pt particle sizes and loading.

The high-angle annular dark-field scanning transmission (HAADF-STEM) images of Pt-CoO/Al_2O_3 and 0.2La-Pt-CoO/Al_2O_3 catalysts after H_2 reduction at 200 °C are shown in Fig. S6. The images of a single particle of the Pt-CoO/Al_2O_3 and 0.2La-Pt-CoO/Al_2O_3 (Fig. 2c-d) show two interplanar distances of 0.23 and 0.19 nm, corresponding to the (111) and (200) planes in face-centered cube (fcc) structured Pt, respectively. The fast Fourier-transform (FFT) patterns (Fig. 2c-d insets) of Pt-CoO/Al_2O_3 and 0.2La-Pt-CoO/Al_2O_3 show the identical features arising from the crystal planes of (200), (111) and (111) of fcc Pt, confirming the existence of metallic Pt in both samples. In these HAADF-STEM images, only Pt particles are formed, and no other metal particles or alloys are discernible in the Pt-CoO/Al_2O_3 and 0.2La-Pt-CoO/Al_2O_3 catalysts. Specially, no lattice fringes of Co- or La-related phases could be observed. In both samples, different elements (Pt, Co and La) are homogeneously distributed on the Al_2O_3 support as revealed by the energy dispersive X-ray (EDX) mappings in Fig. S7.

X-ray photoelectron spectroscopy (XPS) was employed to examine the chemical states of the elements in the catalysts. The La 3d XPS spectrum in Fig. S8a displays two peaks located at 835.3 and 852.8 eV of binding energy, together with two satellite peaks at around 854.4 and 838.5 eV, which can be attributed to the La $3d_{3/2}$ and La $3d_{5/2}$ spin orbits of La_2O_3, respectively [48,49]. The Co 2p XPS spectra of Pt-CoO/Al_2O_3 and 0.2La-Pt-CoO/Al_2O_3 catalysts (Fig. S8b) shows the characteristic features of CoO, i.e., two peaks centered at 795.3 and 781.8 eV arising from the Co $2p_{1/2}$ and Co $2p_{3/2}$ of Co^{2+}, respectively [21,50]. Because the Pt 4 f and Al 2p peaks are overlapped, we used the Pt 4d line to show the chemical states of Pt on the Pt-CoO/Al_2O_3 and 0.2La-Pt-CoO/Al_2O_3 catalysts surface. The main Pt $4d_{5/2}$ peak (Fig. S8c) shows that the binding energy of the metallic Pt phase in Pt-CoO/Al_2O_3 catalysts (314.4 eV) is slightly higher than the 0.2La-Pt-CoO/Al_2O_3 catalysts (314.2 eV) [51], suggesting the electron-rich nature of Pt in 0.2La-Pt-CoO/Al_2O_3, possibly caused by the charge transfer from La_2O_3 to Pt.

3.3. In situ DRIFTS characterization

In situ diffuse reflectance infrared Fourier-transform spectroscopy (DRIFT) characterization was performed to obtain the surface chemistry states of the catalysts by using CO as the probe molecules. Before the DRIFTS characterizations, the catalysts were pre-reduced in H_2 at 200 °C for 30 min and then cooled down to room temperature. The reaction gas was pumped into the reaction cell until saturated adsorption and the DRIFTS spectra were then recorded. As given in Fig. 3a, all the Pt/Al_2O_3, Pt-CoO/Al_2O_3 and 0.2La-Pt-CoO/Al_2O_3 samples display an adsorption peak at ~2040 cm^{-1}, which is attributed to the linear adsorbed CO on Pt clusters (1 −2 nm) [19,52–54], and a peak at ~1815 cm^{-1} that is ascribed to the bridge-adsorbed CO on Pt (111) terraces [55]. Compared with Pt/Al_2O_3, the peak intensity of CO linear adsorption on Pt-CoO/Al_2O_3 and 0.2La-Pt-CoO/Al_2O_3 declines, suggesting the weakened CO adsorption strength on Pt sites in these two samples.

In order to further illustrate the surface chemistry states of Pt species during the reaction, the spectra of DRIFTS (Fig. 3b) were collected under wet COOX reaction condition. In the oxidic atmosphere, both the linear (~2046 cm^{-1}) and bridged (~1820 cm^{-1}) CO adsorption peaks remain, but show a slight shift to the higher wavenumber direction. Notably, the peak intensity of the linearly adsorbed CO on 0.2La-Pt-CoO/Al_2O_3 has dropped sharply, indicating that the CO linear adsorption on 0.2La-Pt-CoO/Al_2O_3 is weaker than on the other two catalysts. Concomitantly, on Pt/Al_2O_3 and Pt-CoO/Al_2O_3, new peaks at 1635 and 1540 cm^{-1} appear which are assigned to the formation of the Pt(CO_3) carbonate species on Pt surfaces. In our previous work, under the dry COOX condition, such carbonate species have never been observed on either the monometallic Pt/Al_2O_3 or the bimetallic Pt-CoO/Al_2O_3 catalysts [21,22]. Hence, the formed carbonate is related to the H_2O during the wet reaction condition (consisting of 1 % CO, 1 % O_2, ~5 % H_2O/Ar) [37,56,57]. The Pt(CO_3) carbonate species block the Pt sites and lead to the water-induced deactivation of the Pt-CoO/Al_2O_3 catalysts under the wet reaction condition, and it could be removed as CO_2 from the catalysts surfaces at elevated temperature [57]. Interestingly, on 0.2La-Pt-CoO/Al_2O_3 the Pt(CO_3) peaks are significantly decreased in intensity, and the relative intensity between the linearly adsorbed the Pt(CO_3) species and CO are 38 %, 39 % and 18 % on Pt/Al_2O_3, Pt-CoO/Al_2O_3 and 0.2La-Pt-CoO/Al_2O_3, respectively, suggesting that the added La_2O_3 can obviously inhibit the formation of carbonate on the Pt sites to enhance the water-resistance under the wet condition [58]. In addition, for the Pt-CoO/Al_2O_3 and 0.2La-Pt-CoO/Al_2O_3 catalysts, there appear two IR peaks at ~2345 cm^{-1} coming from gas phase CO_2 [56]. The strength of CO_2 peaks is much stronger on 0.2La-Pt-CoO/Al_2O_3, consistent with its high catalytic performance for CO oxidation in the wet COOX condition at room temperature.

3.4. In situ XAFS characterization

To further investigate the structure information about the metal species of the catalysts under different conditions, in situ X-ray absorption fine-structure (XAFS) spectra were collected. The in situ Pt L_3-

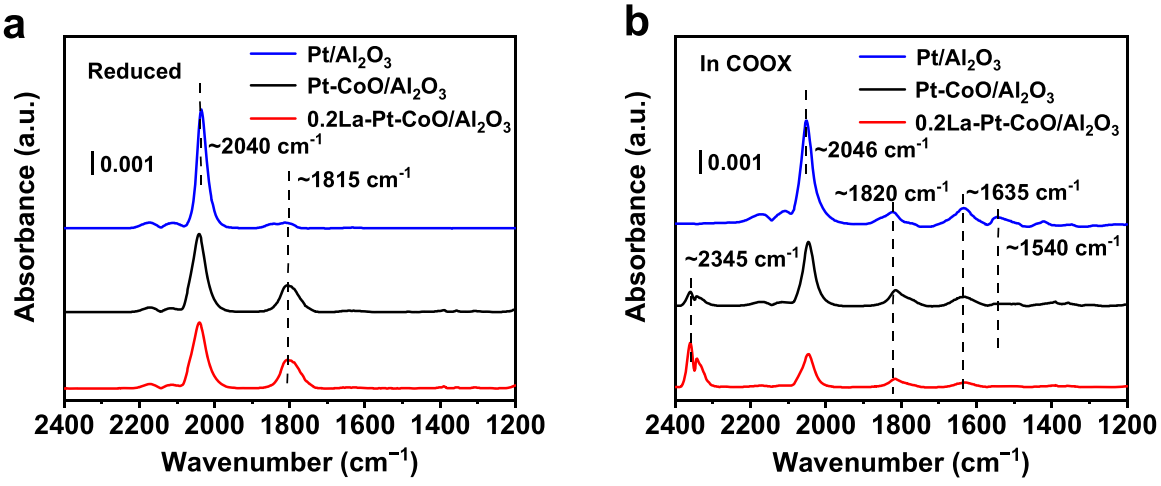

Fig. 3. (a) DRIFTS spectra of various pre-reduced catalysts upon CO saturated adsorption. (b) DRIFTS spectra of various pre-reduced catalysts under the wet COOX condition.

edge XAFS spectra of various catalysts are shown in Fig. 4. The normalized X-ray absorption near-edge structure (XANES) spectra of all the reduced catalysts are displayed in Fig. 4a. The identical spectral shape and the close white line intensity as compared with Pt foil demonstrate that all the Pt atoms of the pre-reduce catalysts are in the metallic states. Furthermore, A close inspection (inset in Fig. 4a) shows that the reduced 0.2La-Pt-CoO/Al_2O_3 catalyst has the lower intensity of white-line than Pt foil, suggesting a higher electron density of Pt in line with the forementioned Pt 4d XPS observations. When the wet COOX reaction gas was injected into the in situ cell, the white-line intensities of all the three catalysts slightly increase (Fig. 4b), and the intensity of the white-line follows the order 0.2La-Pt-CoO/Al_2O_3 > Pt/Al_2O_3 > Pt-CoO/Al_2O_3 (Fig. 4b inset), suggesting the highest oxidation extent of 0.2La-Pt-CoO/Al_2O_3 in all the catalysts.

The normalized Pt L_3-edge XANES spectra under different conditions of a same catalyst are compared in Fig. S10. For the Pt/Al_2O_3 catalyst, a considerable white-line intensity increase under the wet COOX condition is observed in relation to the reduced catalyst (Fig. S10a). In our previous studies [21,22], we have shown that Pt/Al_2O_3 shows no visible change in XANES under the dry reaction condition due to the prohibited activation of O_2 by the strongly adsorbed CO. Therefore, the appearance of the oxidized Pt atoms is connected with the emergence of water-induced carbonate in Pt/Al_2O_3 as revealed by the DRIFT spectra, rather than from O_2 activation [38]. For Pt-CoO/Al_2O_3, Fig. S10b shows that the white-line intensity is marginally increased under the wet COOX condition, even lower than that under the dry COOX condition [21,22]. In combination with the DRIFTS analysis, we speculate that upon exposure to the wet COOX condition, CO_2 was rapidly produced due to the high initial activity of the Pt−CoO interfaces [21,22]. Under the wet conditions, the produced CO_2 molecules react with the water molecules to generate the carbonate that covers the Pt sites and blocks the active Pt−CoO interfacial sites, thus inhibiting the further O_2 activation. On 0.2La-Pt-CoO/Al_2O_3, the DRIFTS results show that very few carbonate species are formed under the wet COOX condition and the CO poisoning is largely weakened; therefore, the O_2 activation on the active sites is permitted. This leads to the largest white-line intensity increase (Fig. S10c) and the highest extent of oxidation of the surface Pt atoms.

Fig. 4c-d shows the Fourier transformed (FT) curves of the Pt L_3-edge extended-XAFS (EXAFS) k^3-weighted $\chi(k)$ functions (Fig. S11) within the k-range of 3.5 − 12.0 $Å^{-1}$ under different conditions. After H_2 reduction, the FT curves of the three samples of Pt/Al_2O_3, Pt-CoO/Al_2O_3 and 0.2La-Pt-CoO/Al_2O_3 exhibit a similar main Pt−Pt peak at around 2.57 Å in the R space, resembling the Pt foil (Fig. 4c). No sign of the formation of the PtCo or other alloys is visible in the FT curves. Under the wet COOX condition, the FT curves of all the catalysts show a new weak peak at around 1.64 Å (Fig. 4d) attributed to the Pt−O bonds, besides the Pt−Pt peak. The Pt–O peak of 0.2La-Pt-CoO/Al_2O_3 is the strongest, consistent with the XANES observations of the highest oxidation extent of Pt therein. To obtain quantitative structural information, the EXAFS curve-fittings were performed by including the Pt−Pt scattering path for the reduced catalysts and both Pt−O and Pt−Pt scattering paths under the wet COOX condition. The fitting results are exhibited in Fig. 4c-d, and the extracted structural parameters are summarized in Table 1 and Table S2. The coordination numbers of Pt−Pt in the reduced catalysts

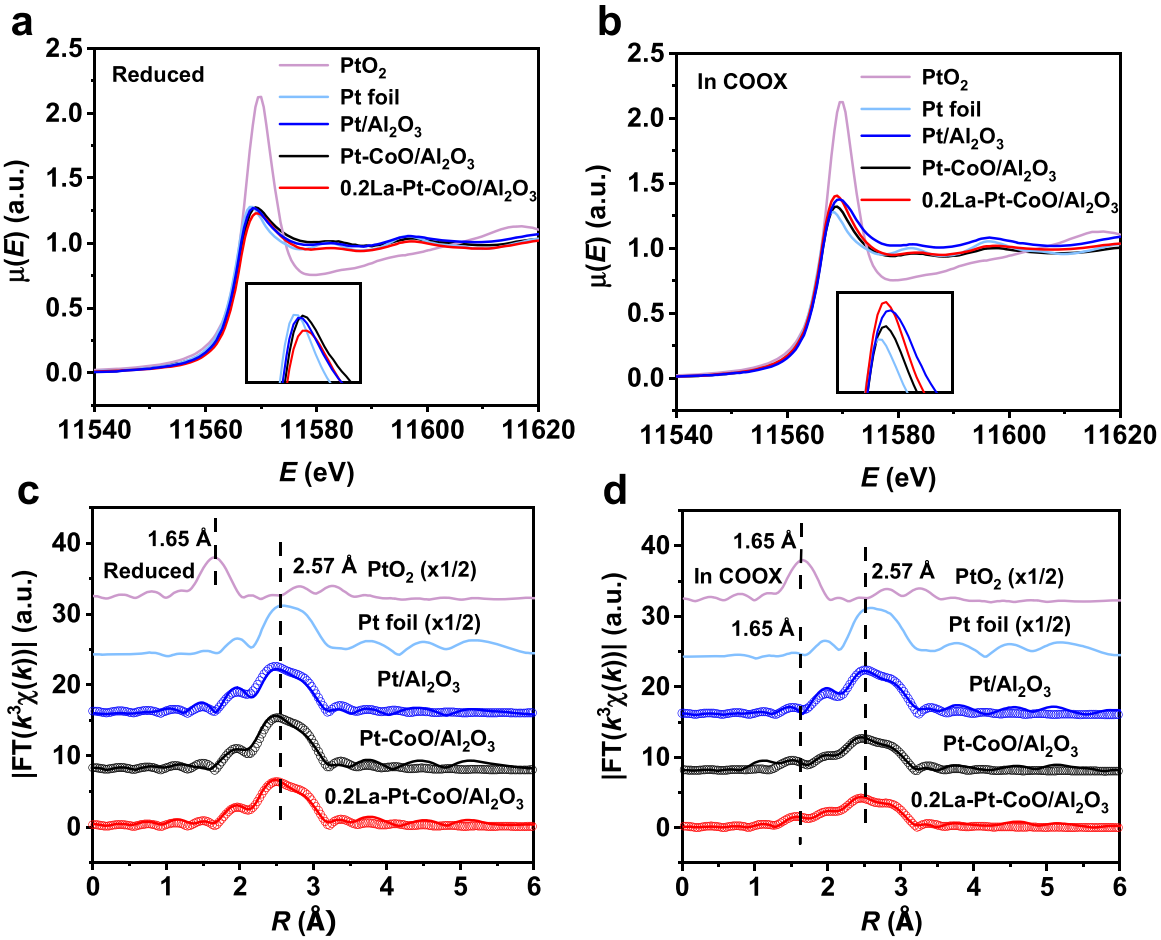

Fig. 4. The Pt L_3-edge XAFS spectra of various catalysts under different conditions. Normalized Pt L_3-edge XANES spectra of (a) the reduced catalysts and (b) catalysts under the COOX condition. The FT curves of the Pt L_3-edge k^3-weighted $\chi(k)$ functions of (c) the reduced catalysts and (d) catalysts under the COOX condition.

are in line with their sizes. Under the wet in situ COOX condition, the coordination number of Pt−O in 0.2La-Pt-CoO/Al_2O_3 (CN_{Pt-O} = 1.0 ± 0.2) is the highest in all samples, indicating that highest oxidation extent of Pt. The Pt−O bonds come from the Pt−O−Co interfacial sites that are active sites for CO oxidation [21,22]. For Pt/Al_2O_3 and For Pt-CoO/Al_2O_3, the Pt−O coordination numbers are very small, due to the formation of water-induced carbonate that covers the Pt sites or blocks the O_2 activation on the Pt−O−Co interfacial sites. Therefore, the strongest Pt−O peak for 0.2La-Pt-CoO/Al_2O_3 suggests the exposure of the Pt−O−Co active interfacial sites, which deliver the high catalytic activity once the water poisoning is inhibited by the La_2O_3 additive.

The in situ Co K-edge XAFS spectra of Pt-CoO/Al_2O_3 and 0.2La-Pt-CoO/Al_2O_3 catalysts are shown in Fig. 5. Seen from Fig. 5a-b, all the Co K-edge XANES spectra of the reduced catalysts and the catalysts under the wet COOX condition resemble that of reference CoO while distinctively different from those of Co foil and Co_3O_4, in agreement with the XPS observations. Meanwhile, the FT curves (Fig. 5c-d) show only a significant Co—O peak at around 1.52 Å, and the next-nearest Co—Co peak in bulk CoO is almost invisible. The Co K-edge XAFS results also indicate that the CoO species is rather stable, regardless of the addition of La or the chemical environment (H_2 reduction or the wet COOX oxidic atmosphere).

4. Discussion

Summarizing the above results, we have demonstrated that the Pt-CoO/Al_2O_3 catalyst, although rather active for catalyzing CO oxidation with a complete CO conversion temperature of 5 °C in 1 % CO and 1 % O_2 atmosphere, is rapidly deactivated by the presence of water vapor. This is in line with numerous previous studies that the interfacial sites between the Pt-group metal and transition-metal oxides could enhance the catalytic activity for dry CO oxidation [20,25,32] but vulnerable to the poisoning of moisture in the reaction gas. As revealed by the in situ DRIFT spectra under the wet COOX condition, this deactivation is cause by the formation of Pt(CO_3) carbonate covering the active Pt−O−Co interfacial sites, in line with numerous previous studies [36,37,59,60]. When the La_2O_3 species is added into the Pt-CoO/Al_2O_3 catalyst, the poisoning effect of H_2O on Pt−O−Co interfacial sites under wet reaction condition is suppressed, due to the surface hydrophobicity of La_2O_3 with unique electronic structure of rare-earth oxides. Moreover, the charge transfer between the La_2O_3 species and Pt makes the Pt in 0.2La-Pt-CoO/Al_2O_3 electron-rich. This helps decrease the CO adsorption strength because of the increased back-donation of Pt 5d to CO 2π* antibonding orbitals [61], and is beneficial for the further improvement of catalytic activity for CO oxidation. As a result, the 0.2La-Pt-CoO/Al_2O_3 catalyst delivers complete CO conversion at −15 °C under the wet reaction environment with further deceased apparent activation energy, and shows a long-term stability under continuous on-stream reaction. We have also shown that too high content of added La_2O_3 decreases the catalytic activity, possibly because the excessive La_2O_3 covers the active sites of the Pt−O−Co interface.

It should be remarked that the La_2O_3 additive plays the main role of water-resistance, but it is intrinsically inert for CO oxidation and its presence alone cannot improve the activity of Pt to a high extent. To manifest this point, we conducted a comparison experiment by adding La into Pt/Al_2O_3 to synthesize the La-doped Pt/Al_2O_3 catalyst (named 0.2La-Pt/Al_2O_3), using the same co-deposition method staring from the 0.2La-Pt colloids. The La content is also approximately 0.2 wt% (Table S1). Fig. S12 shows that 0.2La-Pt/Al_2O_3 possesses the similar catalytic activity with that of Pt/Al_2O_3, i.e., the 100 % CO conversion

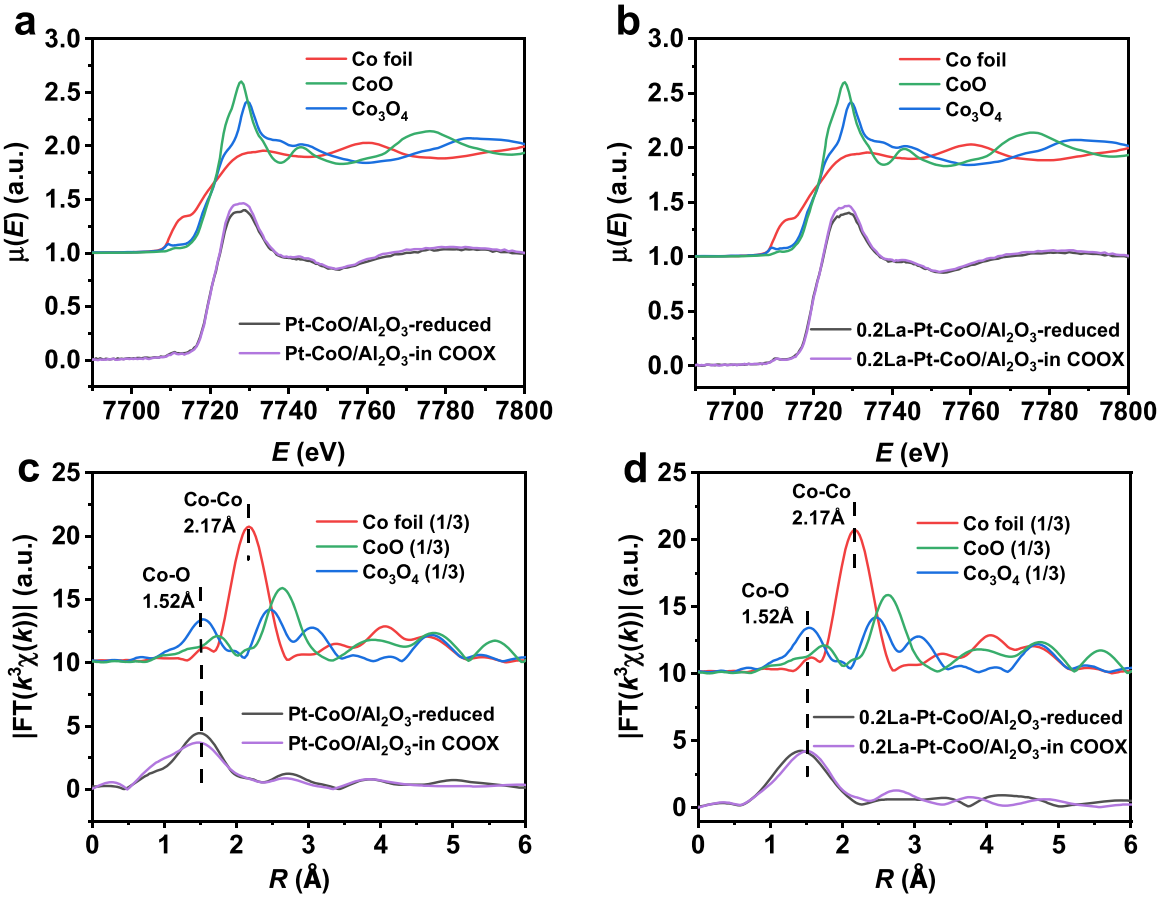

Fig. 5. The Co K-edge XAFS spectra of various catalysts under different conditions. Normalized Co K-edge XANES spectra of (a) Pt-CoO/Al_2O_3 and (b) 0.2La-Pt-CoO/Al_2O_3. The FT curves of the Co K-edge k^3-weighted $\chi(k)$ functions of (c) Pt-CoO/Al_2O_3 and (d) 0.2La-Pt-CoO/Al_2O_3.

could only be achieved at 150 °C. At lower temperatures, 0.2La-Pt/Al_2O_3 exhibits somewhat higher activity than Pt/Al_2O_3. We hypothesize that this may be a result of the La_2O_3-to-Pt charge transfer, which weakens the CO adsorption strength due to the of Pt 5d to CO 2π* backdonation. This is also supported by the in situ XANES spectra of $La_{0.2}Pt/Al_2O_3$ (Fig. S13), as the white-line intensity of the reduced $La_{0.2}Pt/Al_2O_3$ is lower than that of Pt foil. Moreover, under the wet COOX reaction condition, the white-line intensity is nearly unchanged, different from the considerably intensified white-line of Pt/Al_2O_3 under the same condition. Such an observation reinforces our conclusion that the La-doping could inhibit the poisoning effect of H_2O on the surface of Pt.

It has been reported that doping La into Co_3O_4 surfaces could improve the CO oxidation activity of Co_3O_4 under moisture-rich conditions [35]. This shows that the surface electronic states of oxides could be modified to enhance the water-resistance. Since Co_3O_4 is also a widely used oxide support in heterogeneous catalysis, one may wonder if this enhancement could also be achieved on the irreducible support such as Al_2O_3. To test this scenario, we used La to modify the Al_2O_3 support by wetness impregnation, on which the Pt-CoO colloidal particles were deposited. The obtained catalyst, Pt-CoO/0.2La-Al_2O_3, was subjected to the COOX reaction under the same moisture-rich condition. Unexpectedly, Pt-CoO/0.2La-Al_2O_3 shows the worse catalytic activity than the Pt-CoO/Al_2O_3 catalyst, and 100 % CO conversion could only be reached at temperatures higher than 200 °C (Fig. S14). This suggests that adding La into the Al_2O_3 supports cannot contribute to the activity enhancement of the Pt-CoO/Al_2O_3 catalyst. Therefore, it is the synergy between the Pt−O−Co interfacial sites, which are highly active for CO oxidation, and the La_2O_3 species, which suppresses the water poisoning of the active sites, that is mainly responsible for the excellent catalytic activity of CO oxidation under the wet reaction condition.

5. Conclusions

We have synthesized La-doped Pt-CoO/Al_2O_3 catalyst by the co-deposition method in colloidal solutions. Compared with the Pt-CoO/Al_2O_3 catalyst which is rather active for CO oxidation under the dry condition but deactivates rapidly under the wet condition, La-doping could effectively suppress the water poisoning and boost significantly the activity for CO oxidation under the moisture-rich condition. In situ X-ray absorption XAFS and DRIFT spectra revealed that the enhanced activity and water resistance of the La-doped Pt-CoO/Al_2O_3 catalyst is attributed to the addition of La in the form of La_2O_3. The La_2O_3 additive plays dual roles: the first is to suppresses the carbonate formation on the active sites, and the second is to act as electronic structure modifier of Pt. The synergetic effect between La_2O_3 and the active Pt−O−Co interfacial sites in Pt-CoO/Al_2O_3 leads to the outstanding catalytic activity of CO oxidation under the moisture-rich condition. This work demonstrates that La_2O_3 or other rare earth element oxides may aid the design of practical water-resistant metal catalysts.

CRediT authorship contribution statement

X. L. synthesized the catalysts, and performed the catalytic tests and DRIFTS characterization; **X. L., P. Y.** and **S. Z.** performed the XAFS measurements and data analysis; **X. L.** and **S. Z.** co-wrote the manuscript; **P. Y., L. H.,** and **X. R.** managed the XRD, XPS, ICP, TEM, EDX characterization; **S. Z.** instructed the work.

Declaration of Competing Interest

The authors declare that they have no known competing financial interests or personal relationships that could have appeared to influence the work reported in this paper.

Data availability

Data will be made available on request.

Acknowledgements

The authors thank the National Key Research and Development Program of China (No. 2021YFA1500403), the National Natural Science Foundation of China (Grant No. 12075243) for financial support. They also appreciate SSRF and NSRL for the synchrotron radiation beam times.

Appendix A. Supporting information

Supplementary data associated with this article can be found in the online version at doi:10.1016/j.apcatb.2023.122678.

References

[1] X. Song, L. Huang, W. He, C. Liu, F. Hu, Y. Jiang, Z. Sun, S. Wei, Electronic metal–support interactions between Pt nanoparticles and Co(OH)2 flakes for CO oxidation, J. Phys. Chem. C 123 (2019) 10907–10916.
[2] L. Huang, X. Song, Y. Lin, C. Liu, W. He, S. Wang, Z. Long, Z. Sun, In situ observations of the structural dynamics of platinum-cobalt-hydroxide nanocatalysts under CO oxidation, Nanoscale 12 (2020) 3273–3283.
[3] Y. Wang, P. Ren, J. Hu, Y. Tu, Z. Gong, Y. Cui, Y. Zheng, M. Chen, W. Zhang, C. Ma, L. Yu, F. Yang, Y. Wang, X. Bao, D. Deng, Electron penetration triggering interface activity of Pt-graphene for CO oxidation at room temperature, Nat. Commun. 12 (2021) 1–7.
[4] F.C. Meunier, L. Cardenas, H. Kaper, B. Smid, M. Vorokhta, R. Grosjean, D. Aubert, K. Dembele, T. Lunkenbein, Synergy between metallic and oxidized Pt sites unravelled during room temperature CO oxidation on Pt/ceria, Angew. Chem. Int. Ed. 60 (2021) 3799–3805.
[5] K. Zhang, L. Li, S. Shaikhutdinov, H.-J. Freund, Carbon monoxide oxidation on metal-supported monolayer oxide films: establishing which interface is active, Angew. Chem. Int. Ed. 57 (2018) 1261–1265.
[6] L. Qi, M. Babucci, Y. Zhang, A. Lund, L. Liu, J. Li, Y. Chen, A.S. Hoffman, S.R. Bare, Y. Han, B.C. Gates, A.T. Bell, PropanE Dehydrogenation Catalyzed by Isolated Pt atoms in SiOZn-OH nests in dealuminated zeolite beta, J. Am. Chem. Soc. 143 (2021) 21364–21378.
[7] S. Chen, Z.-J. Zhao, R. Mu, X. Chang, J. Luo, S.C. Purdy, A.J. Kropf, G. Sun, C. Pei, J.T. Miller, X. Zhou, E. Vovk, Y. Yang, J. Gong, Propane dehydrogenation on table S1-site [PtZn4] intermetallic catalysts, Chem 7 (2021) 387–405.
[8] Q. Sun, N. Wang, Q. Fan, L. Zeng, A. Mayoral, S. Miao, R. Yang, Z. Jiang, W. Zhou, J. Zhang, T. Zhang, J. Xu, P. Zhang, J. Cheng, D.C. Yang, R. Jia, L. Li, Q. Zhang, Y. Wang, O. Terasaki, J. Yu, Subnanometer bimetallic platinum-zinc clusters in zeolites for propane dehydrogenation, Angew. Chem. Int Ed. Engl. 59 (2020) 19450–19459.
[9] B.F. Zhang, G.Z. Li, S.B. Liu, Y.C. Qin, L.J. Song, L. Wang, X.W. Zhang, G.Z. Liu, Boosting propane dehydrogenation over PtZn encapsulated in an epitaxial high-crystallized zeolite with a low surface barrier, ACS Catal. 12 (2022) 1310–1314.
[10] Y. Li, M. Kottwitz, J.L. Vincent, M.J. Enright, Z. Liu, L. Zhang, J. Huang, S. D. Senanayake, W.-C.D. Yang, P.A. Crozier, R.G. Nuzzo, A.I. Frenkel, Dynamic structure of active sites in ceria-supported Pt catalysts for the water gas shift reaction, Nat. Commun. 12 (2021) 1–9.
[11] M. Yang, J. Liu, S. Lee, B. Zugic, J. Huang, L.F. Allard, M. Flytzani-Stephanopoulos, A common single-site Pt(II)-O(OH)(x)- species stabilized by sodium on "Active" and "Inert" supports catalyzes the water-gas shift reaction, J. Am. Chem. Soc. 137 (2015) 3470–3473.
[12] K. Ding, A. Gulec, A.M. Johnson, N.M. Schweitzer, G.D. Stucky, L.D. Marks, P. C. Stair, Identification of active sites in CO oxidation and water-gas shift over supported Pt catalysts, Science 350 (2015) 189–192.
[13] S.C. Ammal, A. Heyden, Water-gas shift catalysis at corner atoms of Pt clusters in contact with a TiO2 (110) support surface, ACS Catal. 4 (2014) 3654–3662.
[14] M.V. Twigg, Progress and future challenges in controlling automotive exhaust gas emissions, Appl. Catal. B Environ. 70 (2007) 2–15.
[15] H.-J. Freund, G. Meijer, M. Scheffler, R. Schlogl, M. Wolf, Co oxidation as a prototypical reaction for heterogeneous processes, Angew. Chem. Int. Ed. 50 (2011) 10064–10094.
[16] M. Casapu, A. Fischer, A.M. Gaenzler, R. Popescu, M. Crone, D. Gerthsen, M. Tuerk, J.-D. Grunwaldt, Origin of the normal and inverse hysteresis behavior during CO oxidation over Pt/Al2O3, ACS Catal. 7 (2017) 343–355.
[17] A.D. Allian, K. Takanabe, K.L. Fujdala, X. Hao, T.J. Truex, J. Cai, C. Buda, M. Neurock, E. Iglesia, Chemisorption of CO and mechanism of CO oxidation on supported platinum nanoclusters, J. Am. Chem. Soc. 133 (2011) 4498–4517.
[18] X.C. Su, P.S. Cremer, Y.R. Shen, G.A. Somorjai, High-pressure CO oxidation on Pt (111) monitored with infrared-visible sum frequency generation (SFG), J. Am. Chem. Soc. 119 (1997) 3994–4000.

[19] A. Beniya, S. Higashi, N. Ohba, R. Jinnouchi, H. Hirata, Y. Watanabe, CO oxidation activity of non-reducible oxide-supported mass-selected few-atom Pt single-clusters, Nat. Commun. 11 (2020) 1–10.
[20] C.H. Wu, C. Liu, D. Su, H.L. Xin, H.-T. Fang, B. Eren, S. Zhang, C.B. Murray, M. B. Salmeron, Bimetallic synergy in cobalt–palladium nanocatalysts for CO oxidation, Nat. Catal. 2 (2018) 78–85.
[21] Y. Pan, L. Xu, L. Huang, W. He, H. Li, S. Wang, Z. Long, Z. Sun, Identification of active sites in Pt–Co bimetallic catalysts for CO oxidation, ACS Appl. Energy Mater. 4 (2021) 11151–11161.
[22] Y. Pan, L. Xu, W. He, H. Li, W. Chen, Z. Sun, Optimizing the synergy between alloy and alloy-oxide interface for CO oxidation in bimetallic catalysts, Nanoscale 14 (2022) 7303–7313.
[23] W. He, X. Zhang, K. Zheng, C. Wu, Y. Pan, H. Li, L. Xu, R. Xu, W. Chen, Y. Liu, C. Wang, Z. Sun, S. Wei, Structural evolution of anatase-supported platinum nanoclusters into a platinum–titanium intermetallic containing platinum single atoms for enhanced catalytic CO oxidation, Angew. Chem. Int. Ed. Engl. (2022), e202213365 (1 of 10).
[24] M. Vandichel, A. Moscu, H. Gronbeck, Catalysis at the rim: a mechanism for low temperature CO oxidation over Pt3Sn, ACS Catal. 7 (2017) 7431–7441.
[25] Y. Jin, G. Sun, F. Xiong, L. Ding, W. Huang, Water-activated lattice oxygen in FeO (111) islands for low-temperature oxidation of CO at Pt-FeO interface, J. Phys. Chem. C 120 (2016) 9845–9851.
[26] S. Song, Y. Wu, S. Ge, L. Wang, Y. Wang, Y. Guo, W. Zhan, Y. Guo, A facile way to improve pt atom efficiency for CO oxidation at low temperature: modification by transition metal oxides, ACS Catal. 9 (2019) 6177–6187.
[27] Y. Jin, G. Sun, F. Xiong, L. Ding, W. Huang, Hydrogen spillover enhanced hydroxyl formation and catalytic activity toward CO oxidation at the metal/oxide interface, Chem. Eur. J. 21 (2015) 4252–4256.
[28] D.-Y. Wei, M.-F. Yue, S.-N. Qin, S. Zhang, Y.-F. Wu, G.-Y. Xu, H. Zhang, Z.-Q. Tian, J.-F. Li, In situ Raman Observation of oxygen activation and reaction at platinum-ceria interfaces during CO oxidation, J. Am. Chem. Soc. 143 (2021) 15635–15643.
[29] R. Mu, Q. Fu, H. Xu, H. Zhang, Y. Huang, Z. Jiang, S. Zhang, D. Tan, X. Bao, Synergetic effect of surface and subsurface Ni species at Pt-Ni bimetallic catalysts for CO oxidation, J. Am. Chem. Soc. 133 (2011) 1978–1986.
[30] R. Jain, E.S. Gnanakumar, C.S. Gopinath, Mechanistic aspects of wet and dry CO oxidation on Co3O4 nanorod surfaces: a NAP-UPS study, ACS Omega 2 (2017) 828–834.
[31] X.L. Xu, J.Q. Li, DFT studies on H2O adsorption and its effect on CO oxidation over spinel Co3O4 (110) surface, Surf. Sci. 605 (2011) 1962–1967.
[32] J. Kim, H. Choi, D. Kim, J.Y. Park, Operando surface studies on metal-oxide interfaces of bimetal and mixed catalysts, ACS Catal. 11 (2021) 8645–8677.
[33] Z.H. Yao, J.Q. Yang, Z. Liu, B. Shan, R. Chen, Y.W. Wen, Y.L. Li, Synergetic effect dependence on activated oxygen in the interface of NiOx-modified Pt nanoparticles for the CO oxidation from first-principles, Phys. Chem. Chem. Phys. 23 (2021) 8541–8548.
[34] H. Zhu, Z. Wu, D. Su, G.M. Veith, H. Lu, P. Zhang, S.-H. Chai, S. Dai, Constructing hierarchical interfaces: TiO2-supported PtFe-FeOx nanowires for room temperature CO oxidation, J. Am. Chem. Soc. 137 (2015) 10156–10159.
[35] J. Bae, D. Shin, H. Jeong, B.S. Kim, J.W. Han, H. Lee, Highly water-resistant La-doped Co3O4 catalyst for CO oxidation, ACS Catal. 9 (2019) 10093–10100.
[36] H.F. Wang, R. Kavanagh, Y.L. Guo, Y. Guo, G.Z. Lu, P. Hu, Structural origin: water deactivates metal oxides to CO oxidation and promotes low-temperature CO oxidation with metals, Angew. Chem. Int Ed. Engl. 51 (2012) 6657–6661.
[37] M.J. Hazlett, W.S. Epling, Mechanistic effects of water on carbon monoxide and propylene oxidation on platinum and palladium bimetallic catalysts, Catal. Today 360 (2021) 401–410.
[38] H. Jeong, J. Bae, J.W. Han, H. Lee, Promoting effects of hydrothermal treatment on the activity and durability of Pd/CeO2 catalysts for CO oxidation, ACS Catal. 7 (2017) 7097–7105.
[39] M.-T. Zhu, K.-F. Zhang, W.-P. Du, A.-P. Jia, M.-F. Luo, J.-Q. Lu, Highly active and water tolerant Pt/MFe2O4 (M = Co and Ni) catalysts for low temperature CO oxidation, Appl. Catal. a Gen. 619 (2021), 118142.
[40] D. Wu, R. Jia, M. Wen, S. Zhong, Q. Wu, Y. Fu, S. Yu, Ultrastable PtCo/Co3O4-SiO2 nanocomposite with active lattice oxygen for superior catalytic activity toward CO oxidation, Inorg. Chem. 59 (2020) 1218–1226.
[41] G. Azimi, R. Dhiman, H.-M. Kwon, A.T. Paxson, K.K. Varanasi, Hydrophobicity of rare-earth oxide ceramics, Nat. Mater. 12 (2013) 315–320.
[42] A. Mazumder, N. Alangr, S. Sethi, K.N. Prabhu, J. Mukherjee, Study on wettability of plasma spray coated oxide ceramic for hydrophobicity, Surf. Interfaces 20 (2020), 100591.
[43] S. Neumann, S. Grotheer, J. Tielke, I. Schrader, J. Quinson, A. Zana, M. Oezaslan, M. Arenz, S. Kunz, Nanoparticles in a box: a concept to isolate, store and re-use colloidal surfactant-free precious metal nanoparticles, J. Mater. Chem. A 5 (2017) 6140–6145.
[44] M. Newville, IFEFFIT: interactive XAFS analysis and FEFF fitting, J. Synchrotron Radiat. 8 (2001) 322–324.
[45] B. Ravel, M. Newville, ATHENA, ARTEMIS, HEPHAESTUS: data analysis for X-ray absorption spectroscopy using IFEFFIT, J. Synchrotron Radiat. 12 (2005) 537–541.
[46] J.L. Ayastuy, A. Gil-Rodriguez, M.P. Gonzalez-Marcos, M.A. Gutierrez-Ortiz, Effect of process variables on Pt/CeO2 catalyst behaviour for the PROX reaction, Int. J. Hydrog. Energy 31 (2006) 2231–2242.
[47] G. Chen, Y. Zhao, G. Fu, P.N. Duchesne, L. Gu, Y. Zheng, X. Weng, M. Chen, P. Zhang, C.W. Pao, J.F. Lee, N. Zheng, Interfacial effects in iron-nickel hydroxide-platinum nanoparticles enhance catalytic oxidation, Science 344 (2014) 495–499.
[48] M. Uma, N. Balaram, P.R. Sekhar Reddy, V. Janardhanam, V. Rajagopal Reddy, H.-J. Yun, S.-N. Lee, C.-J. Choi, Structural, chemical and electrical properties of Au/La2O3/n-GaN MIS junction with a high-k lanthanum oxide insulating layer, J. Electron. Mater. 48 (2019) 4217–4225.
[49] S.R. Sanivarapu, J.B. Lawrence, G. Sreedhar, Role of surface oxygen vacancies and lanthanide contraction phenomenon of Ln(OH)3 (Ln = La, Pr, and Nd) in sulfide-mediated photoelectrochemical water splitting, ACS Omega 3 (2018) 6267–6278.
[50] H. Qin, X. Qian, T. Meng, Y. Lin, Z. Ma, Pt/MOx/SiO2, Pt/MOx/TiO2, and Pt/MOx/Al2O3 catalysts for CO oxidation, Catalysts 5 (2015) 606–633.
[51] Y. Chen, Y. Feng, L. Li, J. Liu, X. Pan, W. Liu, F. Wei, Y. Cui, B. Qiao, X. Sun, X. Li, J. Lin, S. Lin, X. Wang, T. Zhang, Identification of active sites on high-performance Pt/Al2O3 catalyst for cryogenic CO oxidation, ACS Catal. 10 (2020) 8815–8824.
[52] L. Shi, G.-M. Deng, W.-C. Li, S. Miao, Q.-N. Wang, W.-P. Zhang, A.-H. Lu, Al2O3 nanosheets rich in pentacoordinate Al3+ ions stabilize Pt-Sn CLusters for Propane Dehydrogenation, Angew. Chem. Int. Ed. 54 (2015) 13994–13998.
[53] J. Raskó, CO-induced surface structural changes of Pt on oxide-supported Pt catalysts studied by DRIFTS, J. Catal. 217 (2003) 478–486.
[54] M.J. Kale, P. Christopher, Utilizing quantitative in situ FTIR spectroscopy to identify well-coordinated Pt atoms as the active site for CO oxidation on Al2O3-supported Pt catalysts, ACS Catal. 6 (2016) 5599–5609.
[55] N.P. Lebedeva, A. Rodes, J.M. Feliu, M.T.M. Koper, R.A. van Santen, Role of crystalline defects in electrocatalysis: CO adsorption and oxidation on stepped platinum electrodes as studied by in situ infrared spectroscopy, J. Phys. Chem. B 106 (2002) 9863–9872.
[56] M.A. Newton, D. Ferri, G. Smolentsev, V. Marchionni, M. Nachtegaal, Room-temperature carbon monoxide oxidation by oxygen over Pt/Al2O3 mediated by reactive platinum carbonates, Nat. Commun. 6 (2015) 1–7.
[57] M. Moses-DeBusk, M. Yoon, L.F. Allard, D.R. Mullins, Z. Wu, X. Yang, G. Veith, G. M. Stocks, C.K. Narula, CO oxidation on supported single Pt atoms: experimental and ab initio density functional studies of CO interaction with Pt atom on theta-Al2O3(010) surface, J. Am. Chem. Soc. 135 (2013) 12634–12645.
[58] F. Grillo, M.M. Natile, A. Glisenti, Low temperature oxidation of carbon monoxide: the influence of water and oxygen on the reactivity of a Co3O4 powder surface, Appl. Catal. B Environ. 48 (2004) 267–274.
[59] M. Kang, Catalytic carbon monoxide oxidation over CoOx/CeO2 composite catalysts, Appl. Catal. A Gen. 251 (2003) 143–156.
[60] D. Wang, L. Lin, R. Zhang, R. Mu, Q. Fu, Stabilizing oxide nanolayer via interface confinement and surface hydroxylation, J. Phys. Chem. Lett. 13 (2022) 6566–6570.
[61] P. Bazin, O. Saur, J.C. Lavalley, M. Daturi, G. Blanchard, FT-IR study of CO adsorption on Pt/CeO2: characterisation and structural rearrangement of small Pt particles, Phys. Chem. Chem. Phys. 7 (2005) 187–194.